JOURNAL OF GEOPHYSICAL RESEARCH, VOL. 93, NO. C6, PAGES 6799–6818, JUNE 15, 1988

The Attenuation Rates of Ocean Waves in the Marginal Ice Zone

PETER WADHAMS AND VERNON A. SQUIRE[1]

Scott Polar Research Institute, University of Cambridge, England

DOUGAL J. GOODMAN

British Petroleum Company Ltd., London, England

ANDREW M. COWAN AND STUART C. MOORE

Polar Oceans Associates, Cambridge, England

During field operations in the Greenland and Bering Seas in 1978, 1979 and 1983, a number of experiments were carried out in which wave energy was measured along a line of stations running from the open sea deep into an icefield. Wave buoys in the water and accelerometer packages on floes were the instruments employed, with airborne vertical photography to supply information on floe size distribution. It was found that the decay of waves is exponential, with a decay coefficient which generally increases with frequency except for a roll-over at the highest frequencies. The observations can be fitted reasonably well to a theory of one-dimensional scattering.

1. INTRODUCTION

This paper describes the results of a series of field experiments carried out by Scott Polar Research Institute (SPRI), Cambridge, England, between 1978 and 1983 to measure wave attenuation rates in the marginal ice zones of the Greenland and Bering Seas. Wave-ice interaction is an important phenomenon in these regions because ice breakup due to wave-induced flexural failure is the chief determinant of floe size distribution.

The first measurements of wave decay in the zone of discrete ice floes near an unconfined ice margin were made by shipborne wave recorder [*Robin*, 1963; *Dean*, 1966 reported in *Wadhams*, 1973, 1986]. Later measurements were made by upward-looking echo sounder from a submerged hovering submarine [*Wadhams*, 1972, 1978] and by airborne laser profilometer [*Wadhams*, 1975]. These early experiments all suggested that wave energy decays exponentially with distance, according to an equation of the form

$$E_f(x) = E_f(0)\exp(-\alpha x) \qquad (1)$$

where α is a frequency dependent attenuation coefficient and $E_f(x)$ is the energy density m^2s of a spectral component centred at frequency f at a penetration x (m). This is suggestive of a scattering process [*Wadhams*, 1973, 1975, 1986; *Squire*, 1983] and therefore it is important to have accurate ice geometry data to match the wave data.

In 1978 SPRI began a new series of experiments in which a helicopter was used to visit floes at intervals of a few km in the icefield along the major axis of the incoming wave spectrum. At each site a wave buoy was inserted between floes to measure the local wave spectrum, while the flexural, heave and surge responses of the experimental floe were measured with accelerometers and strainmeters. The thicknesses of the experimental floes were determined by coring, and floe size distributions along the flight path into the ice were derived from overlapping vertical photography done from the helicopter. In this paper we report on the attenuation results from five field experiments of this kind:

1. East Greenland pack ice experiments done in the vicinity of Kong Oscars Fjord (72° N) in September 1978 (Greenland Sea 1978);
2. Experiments done during the cruise of NOAA ship *Surveyor* to the Bering Sea ice margin in March 1979 (Bering Sea 1979);
3. Further experiments in the Kong Oscars Fjord area of east Greenland in September 1979 (Greenland Sea 1979);
4. Experiments done during the MIZEX-West experiment in February 1983 in the Bering Sea, from NOAA ship *Discoverer* and USCG cutter *Westwind* (Bering Sea 1983);
5. Experiments done during the MIZEX-83 experiment in the Fram Strait region of the Greenland Sea (77–79° N) during July 1983, from the Norwegian M.V. *Polarbjørn* (Greenland Sea 1983).

The most recent set of experiments used a directional wave buoy, and have been reported by *Wadhams et al* [1985, 1986].

2. DESCRIPTION OF FIELD EXPERIMENTS

2.1. Greenland Sea 1978

These experiments were carried out at Mestersvig in east Greenland (72° N, 24° W) from which flights were made by Bell 204B helicopter out to the nearby pack ice. Wave energy was recorded using *Seaspri*, a simple free-floating spar buoy with a chain to ballast it and a vertical accelerometer in its head, connected by cable to an FM magnetic tape recorder and amplifier on the ice floe. The vertical photography was done using a Hasselblad camera mounted either

[1]Now at Department of Mathematics and Statistics, University of Otago, Dunedin, New Zealand.

Paper number 7C0705.
0148-0227/88/007C-0705$05.00

in the helicopter itself or in a Twin Otter aircraft. A description of the field operation as a whole is given in *Wadhams* [1979], while *Overgaard et al* [1983] give a general description of the ice conditions at the time of the experiments. Results already reported comprise measurements on an ice island in the fjord [*Goodman et al*, 1980]; and temperature, salinity, density and pH measurements on ice cores [*Overgaard*, 1980; *Overgaard et al*, 1983].

The experiments where a sequence of sites was visited so as to yield wave decay rates were carried out on 16th September (6 stations), 18th (4), 19th (4), 21st (3) and 22nd (5). The locations of the stations are shown in figure 1. Floe size information is available for the 19th, with vertical photography from the helicopter, and for the 18th and 22nd from the Twin Otter.

2.2 Bering Sea 1979

A single wave attenuation experiment was carried out from NOAA ship *Surveyor* in 1979. The experiment is reported in *Squire and Moore* [1980], and a description of ice conditions during the experiment is given in *Squire* [1979] and *Squire and Martin* [1980]. Although no detailed mapping of the ice morphology on the day of the attenuation run took place, an overflight by a NASA Convair 990 a few days later provided a 200 km long aerial photographic run from which characteristic floe size distribution statistics were obtained.

On the day of the experiment the sea ice cover in the MIZ region was of 5/10 concentration and consisted of three zones. The outermost edge zone, extended for 5 km and comprised floes of 20–30 m diameter that had been heavily deformed through inelastic collisions caused by high waves.

TABLE 1. The Eight Floe Stations Making up the Bering Sea 1979 Attenuation Experiment

Floe station	Distance from ice edge, km
1	0.0
2	0.7
3	2.2
4	5.3
5	10.3
6	18.9
7	38.6
8	65.1

A transition zone (5–30 km) had floes of similar diameter which were less deformed; the wave field could still limit floes size by fracture but was not sufficient to cause deformation by collision. In the interior zone (>30 km) the wave energy was insufficient to break up floes, so that large floes greater than 100 m in diameter could be found.

The ship's Bell 206 helicopter occupied eight wave stations on ice floes as shown in table 1. Floes of similar character, of diameter 20–30 m, and thickness approximately 0.5 m, were chosen to ensure that the frequency-dependent heave responses of the floes were roughly comparable [*Squire*, 1981]. At each site a vertical accelerometer was used to measure the heave of the floe; the 20 minute records were amplified and recorded on a TOA chart recorder. For most of the attenuation run a Waverider buoy, borrowed from the Pacific Marine Environmental Laboratory, recorded the incoming wave spectrum in the open sea outside the ice edge. This provided a monitor for the forcing, and a determination of the stationarity of wave conditions for the duration of the experiment (several hours).

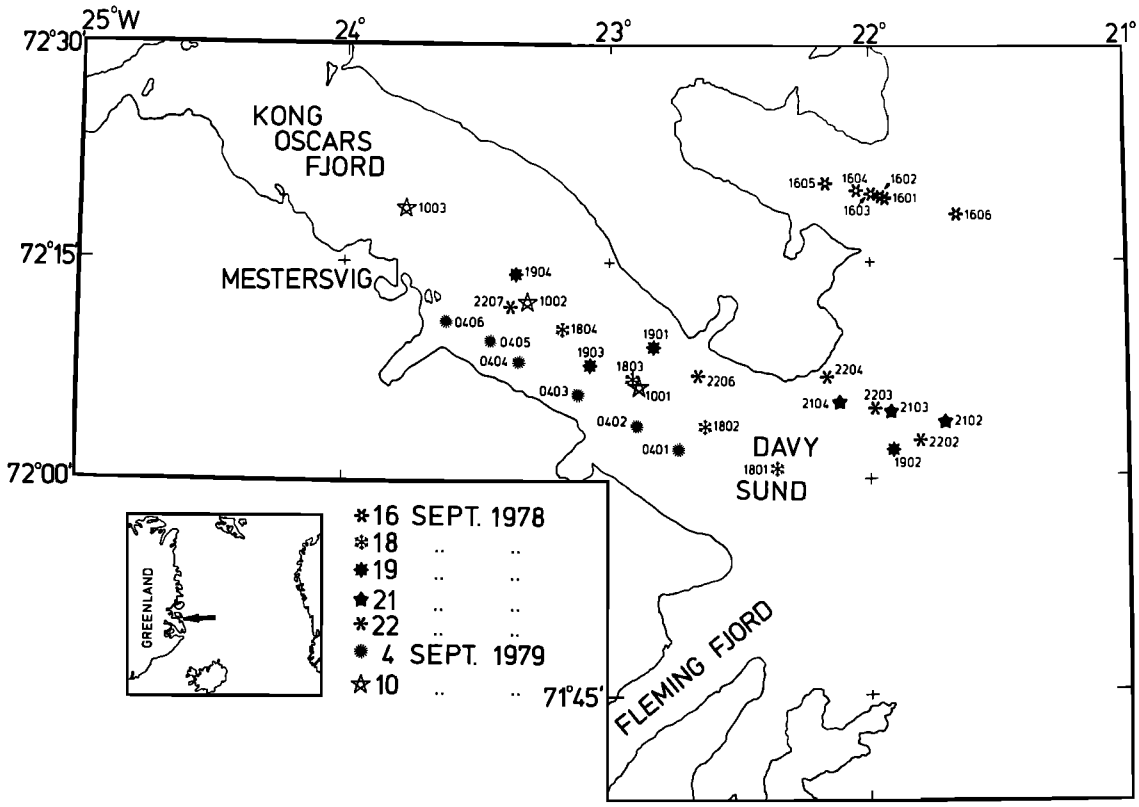

Fig. 1. Wave stations occupied in Kong Oscars Fjord area, east Greenland 1978 and 1979.

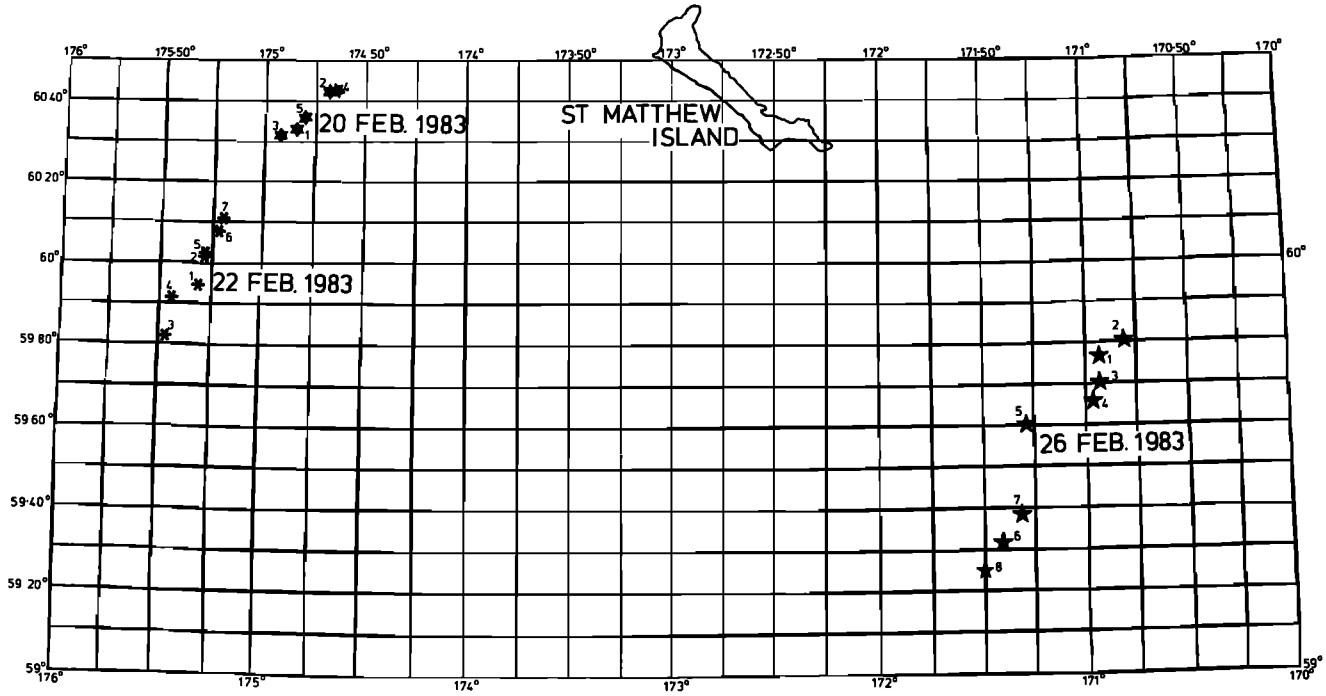

Fig. 2. Wave stations occupied during MIZEX-West experiment in the Bering Sea, February 1983.

2.3. Greenland Sea 1979

These experiments were identical to the 1978 Greenland Sea programme, except that the Hasselblad camera was replaced by a Vinten F95 70 mm reconnaissance camera. Ice was much sparser in the fjord than in 1978. Its properties are again described in *Overgaard* [1980] and *Overgaard et al* [1983]; it consisted mainly of multi-year ice which had been trapped in the fjord during the winter. The main East Greenland pack had retreated further up the coast and was not connected with the Kong Oscars Fjord ice as it had been in the summer of 1978.

Two wave attenuation experiments were carried out. On 4 September six evenly spaced stations were occupied along the axis of Kong Oscars Fjord (figure 1) in a reasonably uniform 3/10 cover of multi-year floes of typical diameter 50–80 m. On 10 September more widely spaced stations were occupied along the fjord axis (figure 1) in a sparser ice cover; some larger floes occurred deeper into the fjord, and floe 1003 was 150 m in diameter.

2.4. Bering Sea 1983

The 1983 Bering Sea field season was part of MIZEX-West, a program to study the marginal ice zone in winter [*Cavalieri et al*, 1983]. Two ships were involved: NOAA ship *Discoverer*, which remained near the ice edge, and USCG cutter *Westwind*, which operated approximately 100 km inside the edge. Early in the experiment four radar transponders were deployed on floes by *Westwind*. Each transponder was accompanied by a *Seadisc*, a disc-shaped wave buoy designed at SPRI by S. C. Moore for use in water or on floes, which employs a gimballed Schaevitz accelerometer to measure vertical acceleration. The buoys were set out in a line of three stretching into the pack ice at 5.6 km intervals with a fourth displaced from the central position. Only the three in-line units are used in the present study. These were located on ice floes of similar character, each of diameter about 20 m. The vertical floe acceleration was telemetered back to *Discoverer* continuously over a 4-day period, and recorded on a Racal Store 14 FM tape recorder. Each sensor was equipped with automatic gain control to optimise its performance in any sea conditions. Two examples of these data were analysed, the first from the beginning of the experiment (7 February), and the second from approximately 12 hours later before the array had seriously deformed. In addition, three further experiments were carried out, all of which were attenuation transects performed using the helicopter to hop from floe to floe. These took place on 20, 22 and 26 February from *Westwind*, with the edge wave conditions and their incident direction measured by *Discoverer*. The incident direction was used to define the baseline for the experiment. The position and relative configuration of floes involved in each attenuation run are shown in figure 2.

2.5. Greenland Sea 1983

Two experiments were carried out from M.V. *Polarbjørn* during the second leg of the MIZEX-83 cruise [*Wadhams et al*, 1981; *Johannessen et al*, 1983]. A preliminary report on the results of SPRI participation in this cruise is given by *Squire et al* [1983].

The first experiment, on July 26, was carried out in a tongue of ice associated with a semi-permanent eddy in Fram Strait (79° N) which has been described by *Wadhams and Squire* [1983]. Figure 3a shows the disposition of the ice and the locations of six sites visited by helicopter. *Polarbjørn* hove to some 4 km outside the ice edge and deployed a *Seadisc* to monitor incoming wave energy. Having ascertained that the main swell was coming from 180°, we ran a line of stations by Bell 206 helicopter as shown along a 33 km baseline; at each station a 22 minute heave record was taken using a vertical accelerometer. Floe size distributions

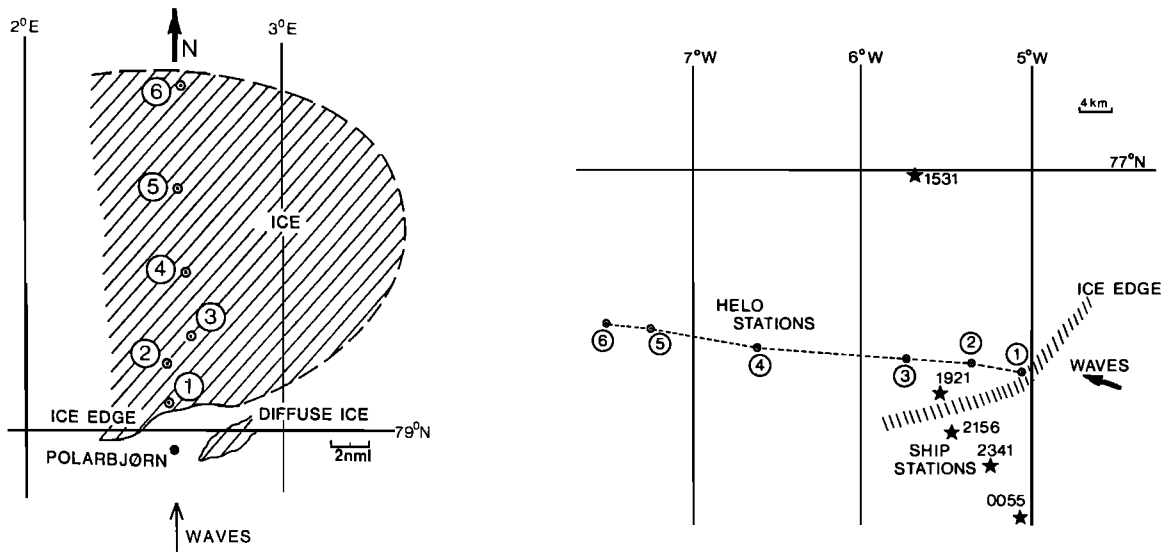

Fig. 3a Fig. 3b

Fig. 3. Wave stations occupied during the attenuation experiments of MIZEX-83 in the Greenland Sea, July 26 and 29 1983.

along the flight line were measured from vertical photography, and each experimental floe was surveyed to estimate its heave response.

The second experiment, on July 29, was carried out at 77 ° N with the ship inside the ice edge. Again six stations were occupied, as shown in figure 3b, aligned along a 53 km baseline in the direction of the incoming swell. Meanwhile the ship, whilst doing oceanographic stations, deployed a *Seadisc* buoy at the locations shown by stars in figure 3b at the times shown; the first location coincided in time with the helicopter stations (1430-1800 GMT). Again, floe size distributions were measured from helicopter photography.

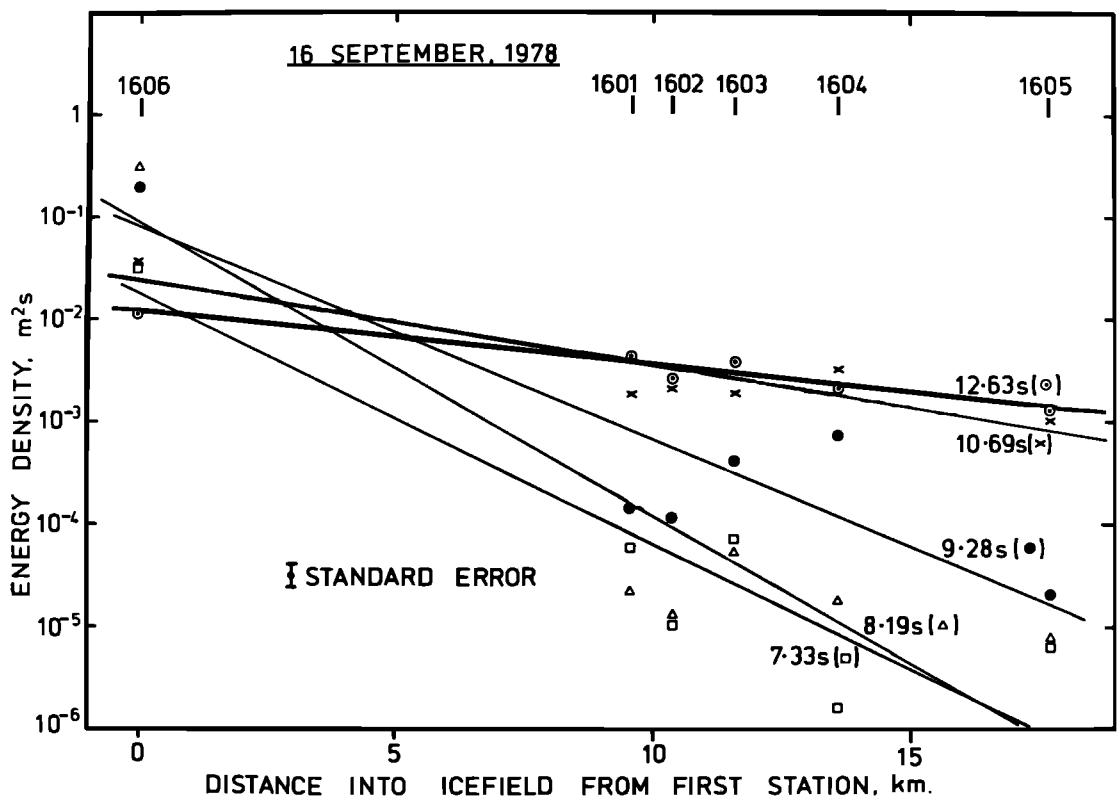

Fig. 4a

Fig. 4. Smoothed energy densities plotted as a function of distance from the ice edge for the 1978 Greenland Sea experiments. Each point is derived from 15 raw energy density values, with a centre period as shown. The lines of best fit for exponential decay are also shown.

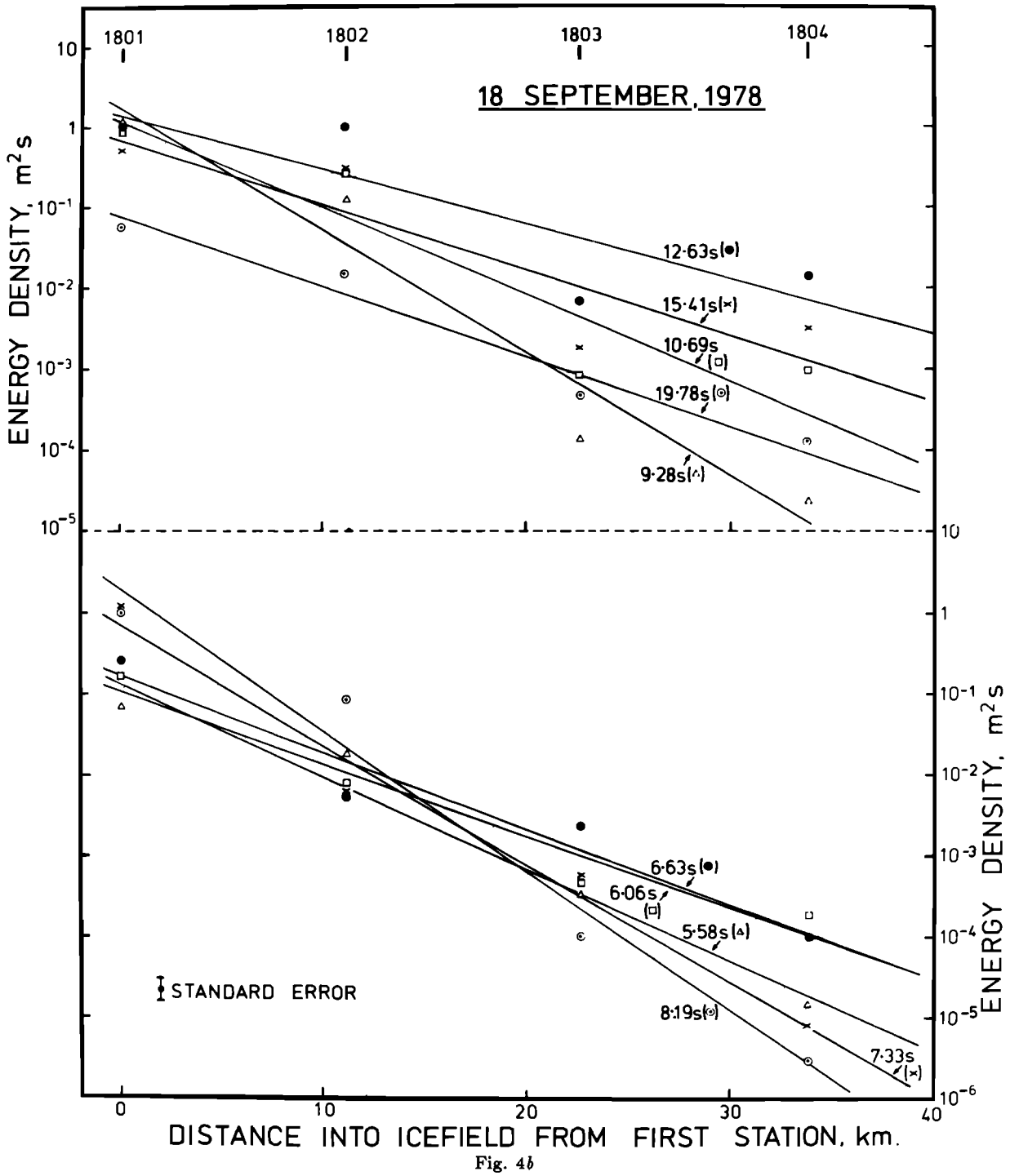

Fig. 4*b*

3. Theory of Wave Decay by Scattering

The problem of floating bodies interacting with ocean waves has received attention because of its relevance to ship motion. The incident wave produces a forced response in the body, and thus generates a scattered wave field. If the body is long compared with its beam, and if it faces a beam sea, the problem reduces to two-dimensions and the scattering is equivalent to a partial transmission and partial reflection of wave energy. Neglecting viscosity and surface tension, and quadratic terms in the body's displacement, we can treat the problem using linear potential theory. This, the simplest approach to wave scattering theory, deals only with attenuation along the line of propagation of a unidirectional wave. Solutions to this problem were first obtained in the case of shallow water, where depth $\ll$ wavelength: *John* [1949] solved for a freely floating cylinder and *Stoker* [1957] for a finite or semi-infinite raft. *Wadhams* [1973, 1986] developed a treatment for floating rafts in deep water which has been found to work well in comparisons with earlier field data [*Wadhams*, 1975, 1978; *Squire*, 1983].

The reader is referred to section B.3 of *Wadhams* [1986] for a description of the theory, which solves for the velocity potential in front of, underneath, and behind an infinitely wide floe of finite length d in the direction of the wave vector. Beneath the floe the surface boundary condition is that

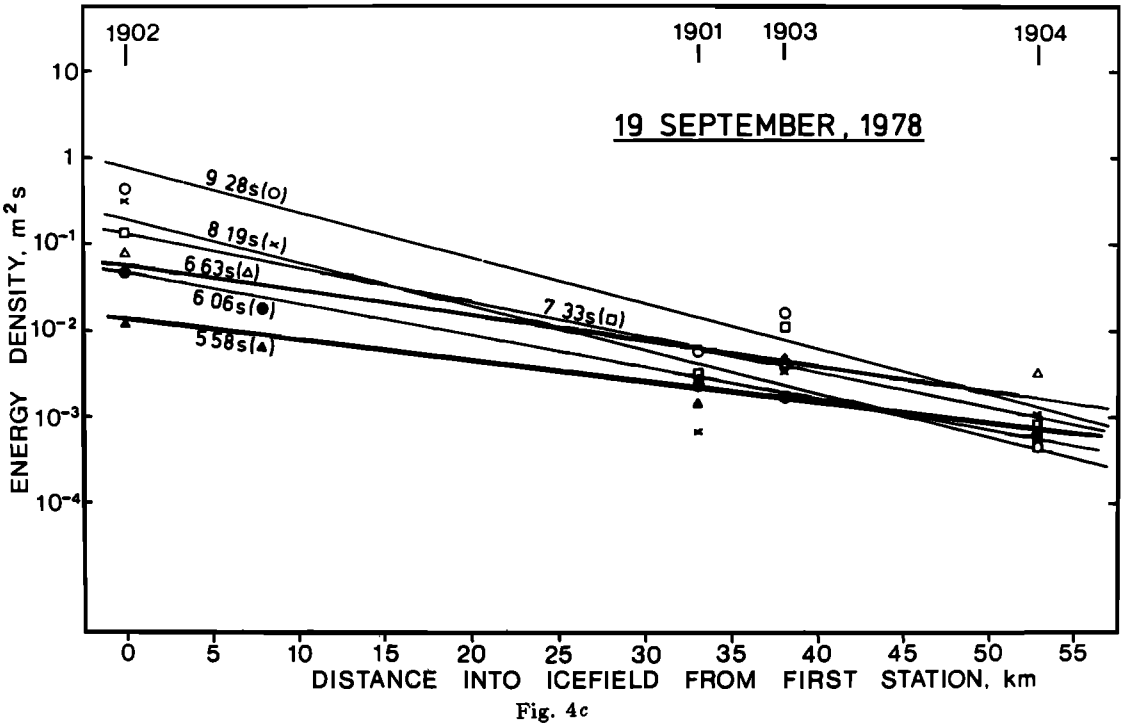

Fig. 4c

the pressure field causes bodily motions of the floe (heave, pitch) and also flexure in the form of flexural-gravity waves obeying the same dispersion relation as similar waves in continuous ice sheets. The three sets of velocity potentials are then matched across the floe edges ($x = 0$ and d). Because the wave number for a flexural gravity wave is different from that of an open water wave of the same frequency, the matching cannot be successful at all depths; it is done at the surface only, to obtain an energy transmission coefficient t ($= |T|^2$) for a single floe. To convert t into an experimental attenuation coefficient α we picture our infinitely long ice floe as equivalent to a row of floes, each of diameter d, situated with their centres at the same value of x so that they all respond in phase to the incoming wave. Energy scattered by individual floes in the positive and negative x-directions is then reinforced, whereas energy scattered to the side is not.

If floes of diameter d occupy a fraction p of sea surface area, there will be p/d equivalent rows per unit penetration in the x-direction. The simplest possible assumption is that only single scattering occurs, i.e. each row transmits a fraction t of the energy incident upon it, while the reflected fraction r is dissipated in an unspecified way before it can get back to the preceding row. Let unit energy per unit area be incident on the ice edge. Then after passing n rows of floes the forward energy is reduced to $E_F = t^n$. Now

$$\frac{\partial E_F}{\partial x} = \frac{p}{d}\frac{\partial E_F}{\partial n} = \frac{pt^n}{d}\ln t \tag{2}$$

The energy attenuation coefficient α for exponential decay is defined by (1), so we have

$$\alpha = \frac{-p\ln t}{d} = \frac{pr}{d} + o(r^2) \tag{3}$$

where $r = 1 - t$ is the energy reflection coefficient. For a real ice field, where floes of size class d_i occupy a fraction p_i of the sea surface area,

$$\alpha = \sum_i \frac{p_i r_i}{d_i} + o(r_i^2) \tag{4}$$

The single scattering approximation is valid if the ice cover is sparse but most ice fields encountered in nature are sufficiently concentrated for multiple scattering to be important. A full treatment of multiple scattering without dissipation predicts that all incoming wave energy is ultimately reflected back out of the front of the icefield, while attenuation within the icefield is linear (A. S. Thorndike, personal communication). Since this is not observed, it is plain that dissipation occurs. A simple treatment which goes one step beyond single scattering is also given in *Wadhams* [1986]. It assumes:

1. A reflected wave vector incident on the far side of a floe experiences the same reflection and transmission coefficients as the main forward wave vector incident on the front.
2. A wave vector is allowed to suffer two reflections and is then dissipated.
3. Energy contributions from individual wave vectors can be added arithmetically, i.e., the scattering is incoherent.

Wadhams showed that these assumptions lead to a modified attenuation rate of

$$\alpha = \frac{p}{d}\left[r - \frac{r}{3+(n-1)r} + o(r^2)\right] \tag{5}$$

where n is the number of rows of floes which the wave has crossed since the edge. Comparison with (4) shows that the effect of multiple scattering is to reduce the observed attenuation coefficient, especially in the outermost parts of the ice field. At the ice edge itself the factor is $2/3$ and it does not begin to increase significantly until we reach a penetration such that $(n-1)r \sim 2 \rightarrow 3$. This corresponds to

$$x \sim 2 \rightarrow 3\left(\frac{d}{rp}\right) \tag{6}$$

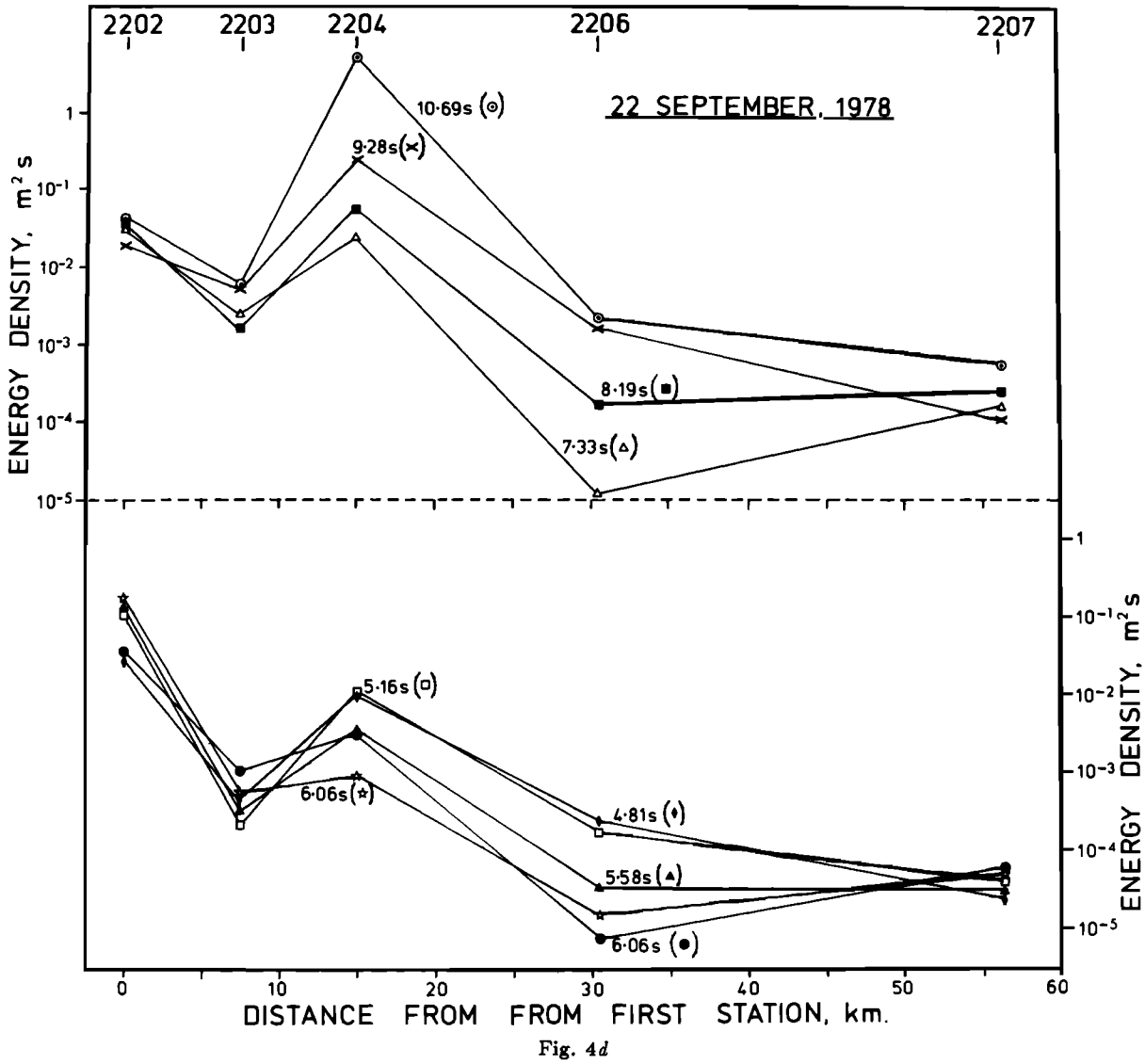

Fig. 4*d*

which in most cases is of the order of km or tens of km. At very great penetrations, α asymptotically approaches its value for single scattering, going as $p(r - d/x)/d$.

Recently an alternative theoretical treatment has been proposed [*Weber*, 1987] which is not based on progressive scattering of incoming waves from ice floes Instead, the ice cover is modelled as a highly viscous Newtonian fluid overlying a slightly viscous (due to turbulent diffusion) rotating ocean. Although originally intended to model brash ice, this second order theory compares favourably with results presented in the present paper for appropriate values of eddy diffusion coefficient.

4. Results

The data from each wave station were digitised and spectrally analysed, with smoothing over 15 contiguous frequency intervals to give a standard error of ±25.8% in each spectral estimate. Each independent smoothed spectral component from the stations in an attenuation run was then plotted as a function of penetration into the ice. In all of the experiments reported in this paper the line of stations was run in the direction of the main component of the sea as judged by eye, so that the penetrations in these plots represent distance measured along the wave propagation vector. The plot of energy density against distance was then subjected to a least squares exponential curve fit so as to determine an attenuation coefficient α of best fit to the data. The values of α calculated in this way are presented in a second plot for each experiment, and are also listed in table 2, together with a standard error (from the goodness-of-fit of the data to an experiment); the frequency interval concerned; and the centre period of that interval. A sample spectrum is also usually shown superimposed on the second plot as an indication of the frequencies at which significant energy is present.

Where the energy density in the spectrum is very small, we expect that a noise level may become important, composed of side lobe leakage from higher energy components, errors due to over-amplification of very small accelerations, and genuine noise in the ocean wave record due to factors such as collisions between floes, wave reflections off the fjord sides etc. We decided that an energy density of 0.01 m^2s in the incident spectrum should be a lower limit for the input signal, and likewise that energy densities in the interior of less than 10^{-5} m^2s should be treated with reserve as being

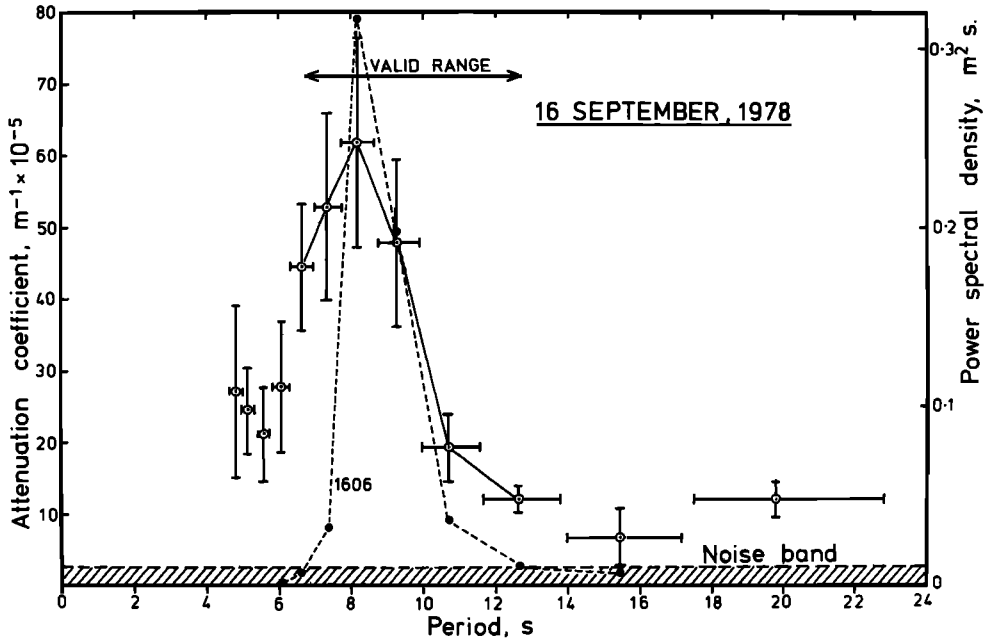

Fig. 5*a*

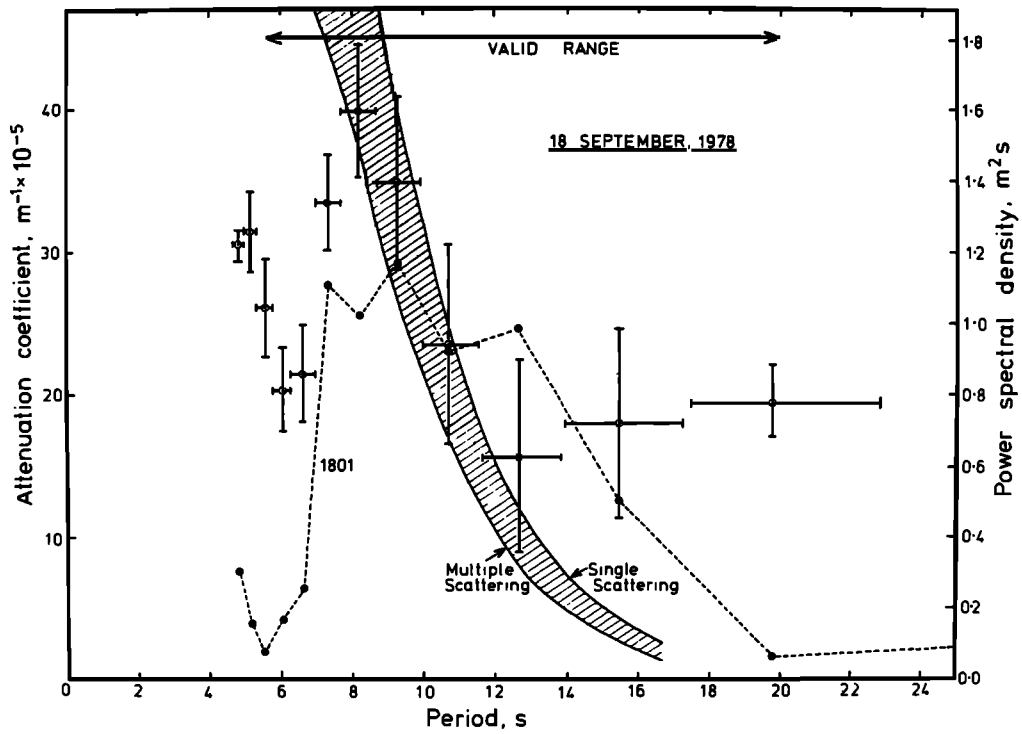

Fig. 5*b*

Fig. 5. Decay coefficients derived from exponential curve fitting of data in figure 4 plotted against period. The energy spectra nearest the ice edge are also shown (right hand scale) on each plot.

likely to consist mainly of noise. This defined the limits of a valid range of periods over which we could calculate the attenuation coefficient.

For every experiment in which concurrent floe size information was available from aerial photography, the model of *Wadhams* [1986] was run using distributions of floe diameters found from analyses of the photographs whereby every floe along the line of overlapping frames was digitised using a curve follower. The thicknesses used in the model runs depended on the experiment location. For the East Greenland data a floe thickness of 3.1 m was used, based on an average of cores taken in Kong Oscars Fjord. In the Bering Sea model runs the floes were distributed among the following thickness categories: 0.4 m, 20 %; 0.7 m, 40 %; 1.1 m, 0 %; 1.7 m, 10 %. These were derived from the results of the extensive coring programme done during the MIZEX-West experiment. Sensitivity studies show that α varies approximately linearly with thickness h, so that errors in thickness

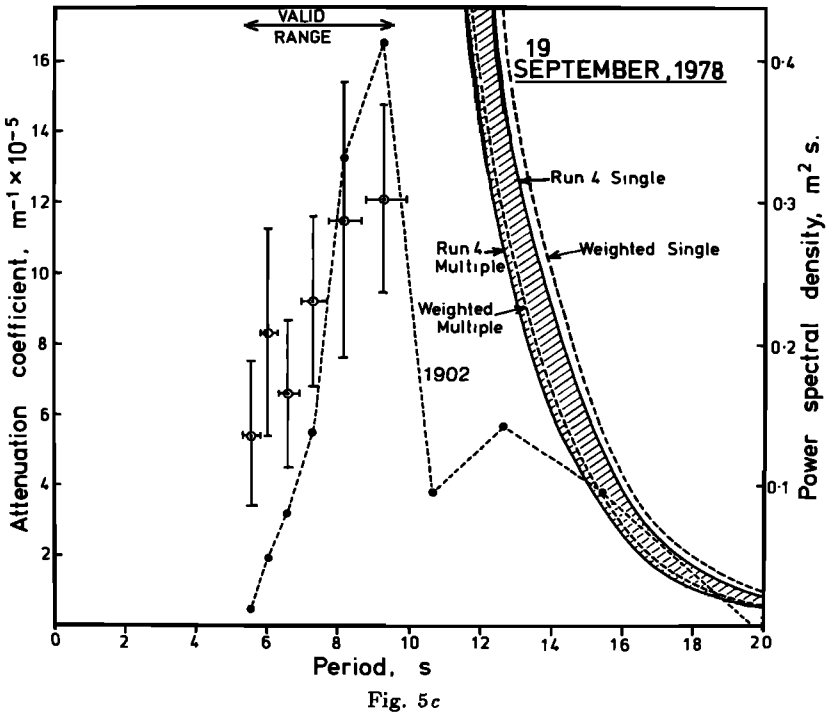

Fig. 5c

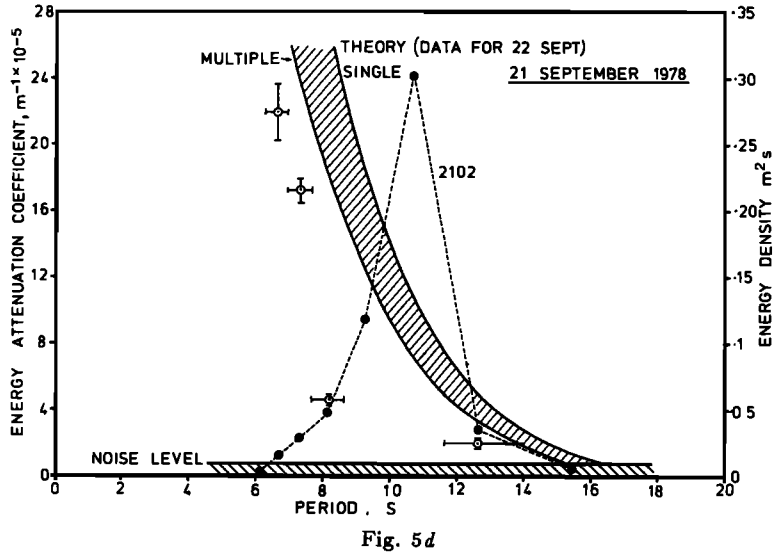

Fig. 5d

measurement are not as crucial as errors in diameter measurement.

In each case the model's predictions of α for single and multiple scattering were computed, and added to the plot of observed α against T. The pairs of model curves are connected by hatching to show the span of the model predictions. The goodness of fit of the model predictions to the observations is then the test of the model's validity.

4.1. Greenland Sea 1978

16 September. The record length used was 1048.1 s and digitising interval was 0.512 s. Figure 4a shows the decay against distance and 5a shows α against T. The spectrum from station 1606, nearest the ice edge, has been added to figure 5a; it is narrow with a peak at 8.4 s period. In figure 5a the horizontal error bars on α represent the range of wave periods covered by the frequency smoothing of each component.

The attenuation rate shows a general increase with frequency; except for a roll-over at the shortest period which will be found to recur in other observations described below. No direct comparison with theory is possible because no aerial photography was carried out, although it was observed that the close ice cover was composed of uniformly sized multi-year floes.

18 September. Two photo-transects were flown by Twin Otter over the experimental area. Ice conditions were far from uniform; this is shown very clearly on a Landsat image taken on that day [figure 3 of *Overgaard et al*, 1983] which demonstrates that there was a gyre within the fjord. This gyre moved ice-free water from the inner part of the fjord out along the southern shore and then mixed it across the width of the fjord in the form of an eddy. The result was

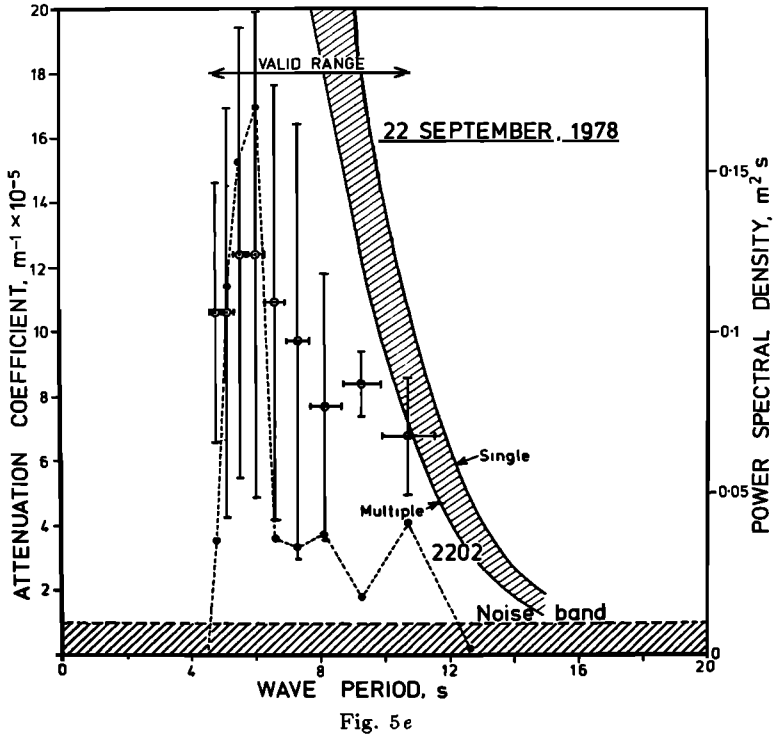

Fig. 5e

that station 1803, on the seaward rim of the eddy, was situated in heavier ice than stations 1801 and 1802, while the space between 1803 and 1804 was partly occupied by the open water of the eddy. The corresponding photo transects were subdivided into six sections, corresponding to distinct zonations in the ice characteristics. Brash and young ice were not included in the analysis. Figure 6 shows the distributions of floe diameters, measured in the direction of the incoming swell. These are very typical of floe size distributions in the outer MIZ. This procedure was undertaken for all subsequent data sets reported in this paper, but we show only this flight analysis as an example of the data used in the model.

Figure 4b shows the energy decay; it can be seen that station 1804 has anomalously high energies and 1803 anomalously low, in relation to 1801 and 1802. The fact that the attenuation run was entirely carried out within the fjord is also a source of uncertainty, due to the possibilities of wave reflection or absorption at the fjord sides. Nevertheless, exponential curve fitting was attempted, with the results shown in figure 5b. The associated wave spectrum from station 1801 superimposed on figure 5b shows that the incoming energy was much greater than on 16 September and spread over a wider range of frequencies. In fact, it never drops below 0.01 m^2s; instead, it reaches minima at low and high frequencies from which it rises again (these were used as the limits of a valid frequency range).

The decay rates within the valid frequency range show the same trends as for 16 September, although the absolute values are lower. Theoretical attenuation rates were computed from the floe size data of the two flight lines, and a mean weighted by track length was used in figure 5b. Observed decay rates lie within the range of computed decay rates for wave periods between 8 s and 11 s where wave energy is highest. At short periods there is a roll-over where the observed decay is much lower than the model predicts, while at long periods the observed attenuation is greater than predicted.

19 September. The four stations (figure 1) were not optimally arranged for attenuation; stations 1901 and 1903 were close together on opposite sides of the fjord, and each may have experienced different effects from wave energy reflected off the fjord sides. Station 1902 was situated near the extreme ice edge in a region of diffuse ice cover. The photographic transect showed that the floes were intermixed with heavy concentrations of brash and thin ice in the outermost 13 km. On the basis of an observed wave direction along the axis of the fjord, attenuations were computed as for previous days. Figure 4c shows the decay against distance; at very long periods actual wave growth was observed, suggesting wind action in the fjord and throwing some doubt on the validity of the other decay rates shown in figure 4c. Figure 5c shows the α plotted against T; the values are low in absolute terms and display the short period roll-over.

The four flight lines gave total concentrations of 19%, 52%, 52% and 41%, sufficiently high for multiple scattering to be important. The fourth flight line corresponded most closely to the experimental line, so computations were made for this line and for a weighted sum of the lines. The results predict a much greater decay rate than is seen in the valid range of 5–10 s period, suggesting that wave growth was indeed important.

21 September. Only three of the day's wave stations produced useful data. However, these were spaced evenly in a line along the observed direction of the major wave vector (figure 1, stations 2102-4), and so it is worthwhile to compute the attenuations observed. Figure 5d shows α values. The incident spectrum was narrow (2102 is shown in figure 5d), and in the frequency range with maximum energy (9–12 s period) wave growth occurred rather than attenuation. As can be seen from figure 1, the station line lay close to a lee shore, so it is very likely that wave reflection was occurring from the coast and giving additional energy to the

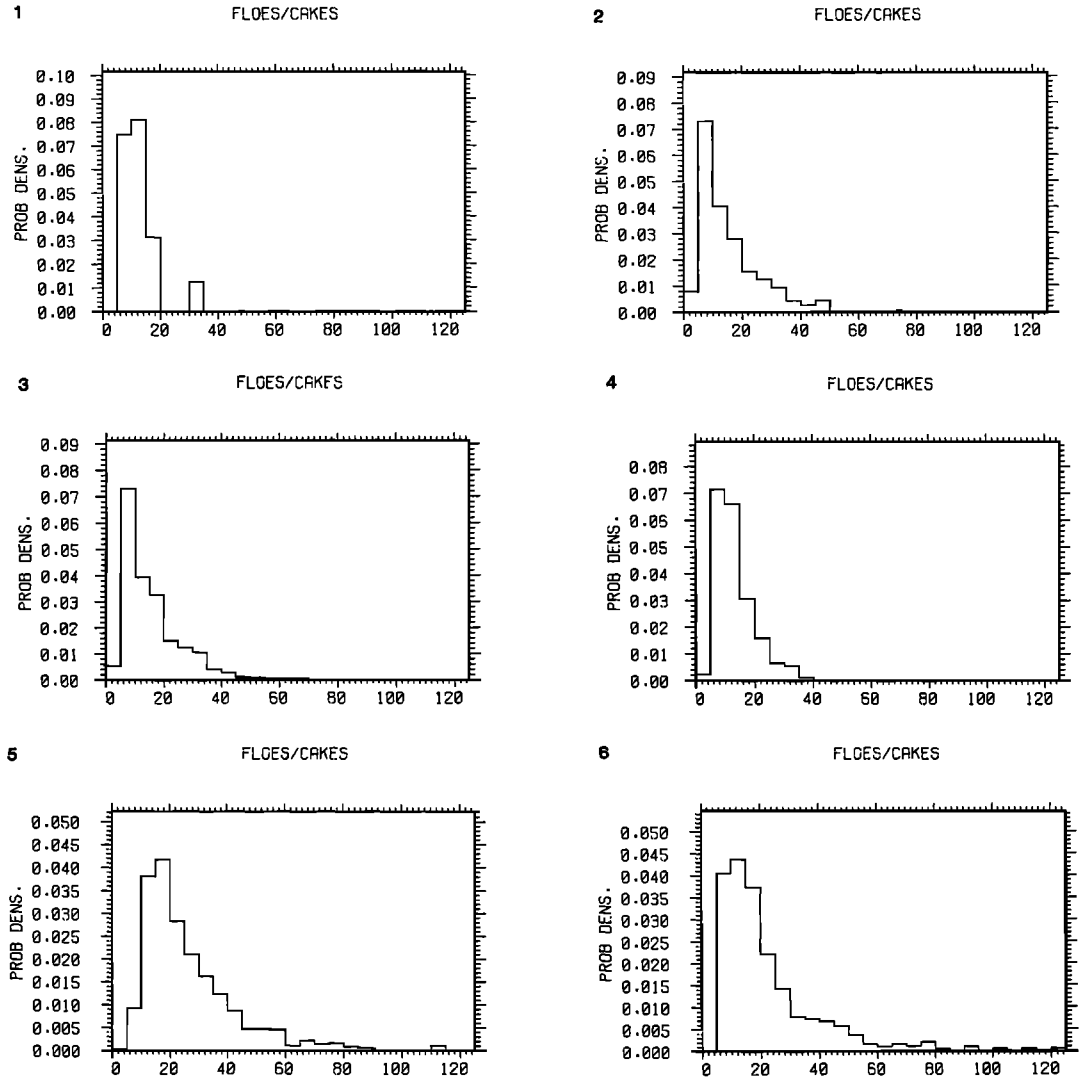

Fig. 6. Probability density functions of floe diameter, measured along swell direction, derived from flight lines of 18 September 1978. Section 1 lay 0 to 3.5 km from ice edge, overall ice concentration 153.5-18.8 km, 1022-26.6 km, 6032.3-34 km, 20

inner stations. In matching the data to the model (figure 1) the same floe size distribution was used as was observed on the 22nd.

22 September. Of the five stations occupied on this day (figure 1), the first three (2202-4) lay in a line incident on a lee shore, allowing the possibility of at least the innermost station 2204 being corrupted by reflected wave energy. The final two stations lay within Kong Oscars Fjord and thus not on a direct line with the first three; we have to assume that a unidirectional wave field was incident on the coast on a wide front. There was a dense ice cover composed not only of high floe concentrations but also of much young ice and brash.

The observed attenuation rates (figure 4d) clearly show the anomalous behaviour of station 2204, where the energies in every case are greater than for the seaward station 2203. We conclude that nearshore reflection and/or wave focussing effects are so strong in station 2204 as to negate the validity of its data. Therefore, in calculating attenuation rates we have used only the four stations 2202, 2203, 2206, 2207. The results are shown in figure 5e.

The flight line most relevant to the experimental line gave a total ice concentration of only 11 %, which indicates that single scattering is most likely. The results, however (figure 5e), give a predicted attenuation rate which is higher than the observed rate.

4.2 Bering Sea 1979

The eight 1200 s heave records were digitised at 0.5 s. The 1200 s Waverider buoy magnetic cassette tapes were digitised at the same rate and spectra (for equivalent time intervals) were calculated. These spectra are plotted dashed in figure 8. The figure indicates that the wave climate changed little during the attenuation experiment, and that the sea off the ice edge was significant only in the 4.5 s to 17 s band when the 0.01 m^2s noise criterion is adopted. Within this range all the spectra are twin-peaked at 12 s and 8 s period.

Figure 7 shows the decay as a function of distance. The fit of the data to a negative exponential is good and shows the predicted increase in the decay rates as the wave periods become smaller.

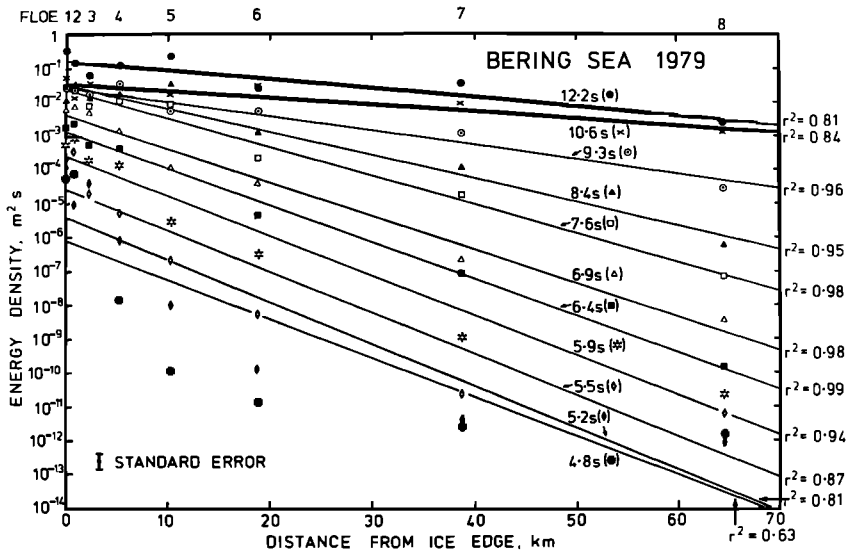

Fig. 7. Energy densities, 1979 Bering Sea experiment.

Figure 8 shows α plotted against T. Within the valid range defined previously, we note the clear and systematic decrease in α as the wave period increases. The fit between theory and observation is good, except for the theory not predicting the roll-over at short periods. The high overall ice concentration indicates that multiple scattering is important.

4.3 Greenland Sea 1979

4 September. Records from the six regularly spaced stations (figure 1) were analysed in 1164.2 s lengths. Figure 10a shows that the incident wave spectrum was narrow, with a peak at 10.5 s period, and a valid range extending from 8 to 14 s. Within this range the decay of each spectral component approximate to a negative exponential (figure 9), and decay rate increased with increasing frequency. The only exception was the component centred on 8.14 s period, which decayed rapidly and exponentially over the first five stations, but at station 0406 exhibited an increase in energy. We ascribe this increase to wave regeneration due to wind blowing up the fjord; we expect this effect to be greatest at short wave periods, and examination of periods less than the valid range shows energy growth. We therefore use only the outer 5 stations for an exponential curve fit to the 8.14 s component (table 2, figure 10a). Note the small standard deviations in all of these attenuation estimates, except at the longest period where, as figure 9 shows, the error is due to the decay rate itself being almost imperceptible.

Concurrent helicopter photography over the floes was obtained on this day, and was analysed as three 10 km bands. The fit with observations across the bands and for their weighted mean is excellent (figure 10a) when single scattering is used.

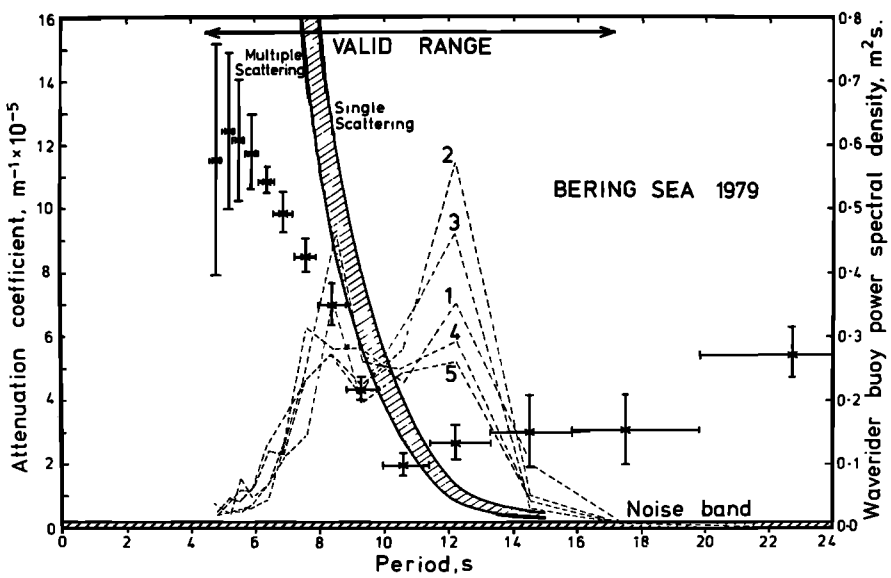

Fig. 8. Decay coefficients and five independent spectra from Waverider buoy in open sea off the ice edge, 1979 Bering Sea experiment.

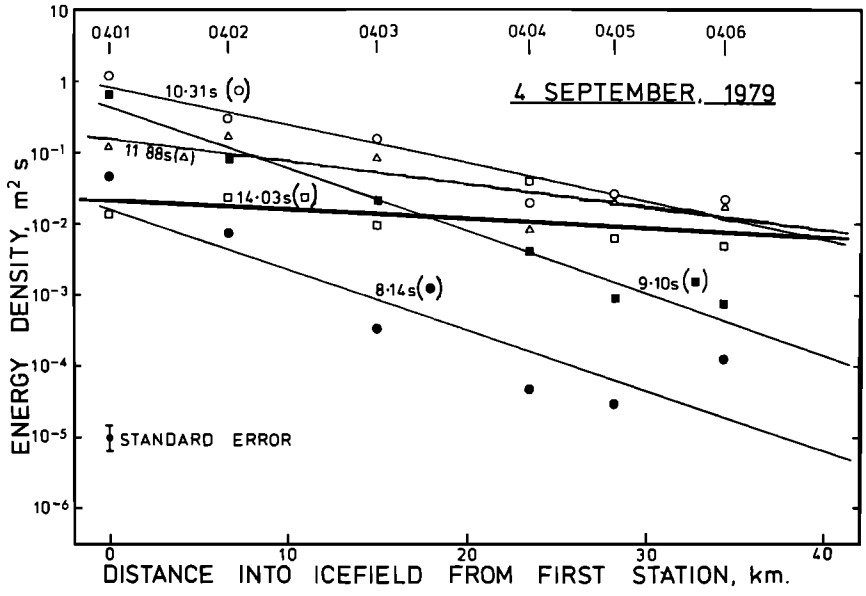

Fig. 9. Energy densities, 4 Sept. 1979.

10 September. Three widely spaced stations were occupied along Kong Oscars Fjord (figure 1). The only deviation from a diffuse ice cover occurred between 17.6 and 23.5 km, where floes were surrounded by brash. Noting also the small number of stations, this suggests that the results should be treated with caution since local effects may dominate. Figure 10b shows the computed attenuation rates, and also shows the spectrum from station 1001. The spectrum displays an increase in energy at very long periods; we suspect that this is an artefact of the recording, so valid range is restricted to periods from the low-period energy minimum (6 s) to 12 s. The results take the familiar form of an increase in decay rate with decreasing wave period, with roll-over at the shortest periods, although errors are large at this end of the spectrum.

Again, concurrent photography was directly over the line of floes. The photographs were analysed in six sections, with total ice concentrations ranging from 2 % to 17 %. The weighted mean α predicted by the model for the sections is plotted in figure 10b for single scattering. Again there is a good fit with observation over the whole valid data range, except at very long periods, where the energies were too low for the observed α to be valid.

4.4 Bering Sea 1983

7 February. Power spectra were derived from the *Seadisc* heave data and used in an exponential curve fit (not plotted). The derived attenuation coefficients are plotted as functions of period in figs. 11a (from the beginning of the buoy deployment) and 11b (from 12 hours later). There is a familiar decrease in α with increasing period, together with a roll-over at short periods. In both cases the spectrum plotted on the figure as a dotted line is that seen by the outermost wave buoy during the experiment; this is not quite the forcing sea wave energy, since the buoy was some 6 km from the ice edge and was located on an ice floe.

The photographic transect was closer in time to experiment 2 than experiment 1 so the results of the model run have been plotted on figure 11b. Total floe concentration in the segments analysed was 59 %–86 %, with the remainder of the sea surface covered with closely packed brash and floe fragments, so multiple scattering is likely to be important. The results show a good fit, except again for a failure to model short period roll-over.

20 February. The first helicopter attenuation transect comprised five stations situated at 4.8 km, 8.2 km, 17.8 km and 19.7 km from station 1 along a bearing of 244 °. The entire array was some 50 km from the ice edge, where *Discoverer* monitored incident waves using a *Seadisc* buoy. The data therefore represent the local wave spectrum and its decay well inside the pack, but with supporting data on the ocean wave activity at the ice edge. The character of the ice cover was markedly different from that encountered on 7 February with large conglomerate floes composed of discrete thick floes welded together with younger ice. Along-track open water stretches contained large patches of very thin ice.

20 minutes of vertical acceleration data were collected at each site. Power spectra for each station and for the ice edge time series were used to compute α (figure 12a), showing the usual decrease between about 10 s and 16 s, a roll-over at short periods, and an increase at longer periods. The three ice edge spectra also plotted in the figure illustrate a gradual change in sea state as the experiment progressed; to 95 % confidence, however, the wave forcing was essentially stationary. The form of the energy spectra was particularly interesting since they show significant energy at around 17 s, which is not found in the interior data. A secondary peak in the open sea spectra occurred at approximately 12.5 s, which is seen in the interior data. It is probable that the long period peak represents swell propagating on a bearing other than that along which the interior sites were positioned. The values for α show large errors (table 2) due to the small number of stations incorporated in the analysis, their close proximity, and possible drift experienced by the ship during the experiment.

Concurrent aerial photography covered a swath connect-

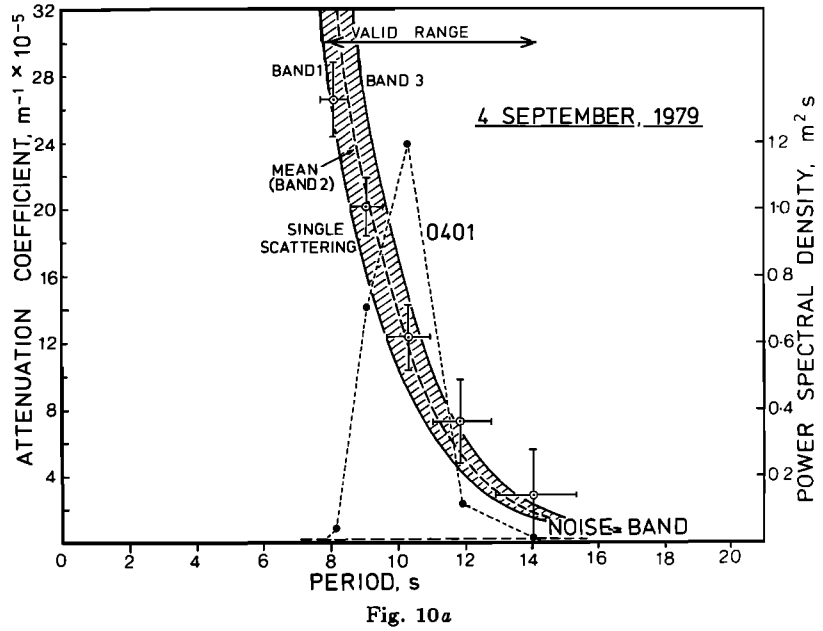

Fig. 10*a*

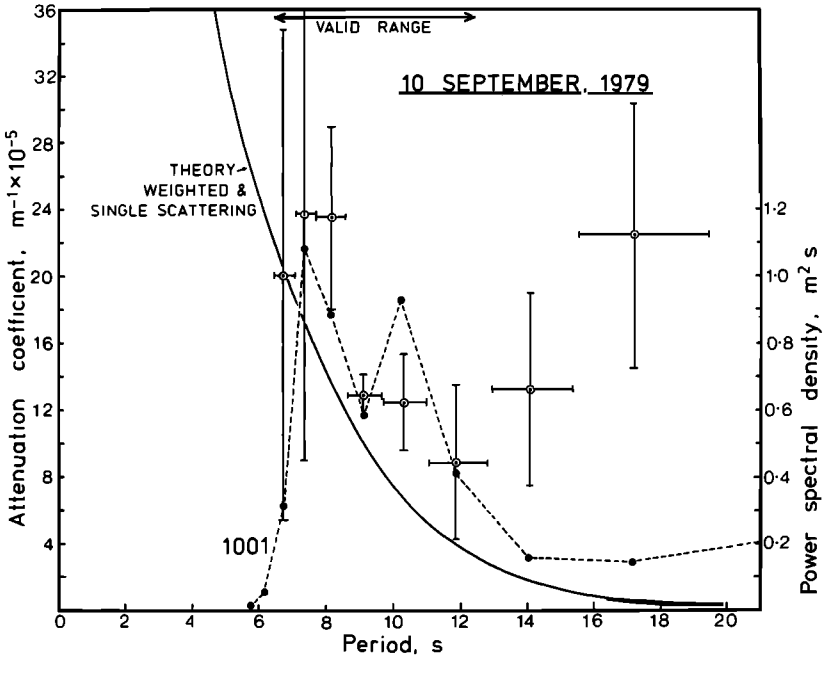

Fig. 10*b*

Fig. 10. Decay coefficients and outermost wave spectra, 4 and 10 Sept. 1979.

ing the sampled floe sites. Overall ice concentration varied between 6 and 34%. The modelled values of α for both single and multiple scattering are plotted in figure 12a, where the fit with observation is especially good (within the valid range) for the single scattering curve. The low ice concentration makes this the more appropriate curve to consider.

22 February. The second helicopter attenuation experiment comprised seven sites along a line 225° located at 10.3 km, 16.7 km, 25.1 km, 25.5 km, 32.1 km and 36.1 km from the most southerly station. Ice edge wave conditions were monitored by *Seadisc* as before. Attenuation coefficients are plotted in figure 12b, together with three ice edge power spectral densities. The same characteristic shape is seen in the curves, with α decreasing with increased wave period within the valid range band (10 s to 18 s). In this case the errors are small due to the large number of stations involved in the study.

26 February. Wave energy was measured along 230° at eight sites located at 10.6 km, 20.0 km, 38.8 km, 56.4 km, 62.0 km, 68.6 km and 74.3 km from the southernmost station in the array. The attenuation coefficients are plotted in figure 13 and given in table 2, and show the same roll-over at short periods, followed by a decreased decay with increasing period and by a gradually increasing decay at

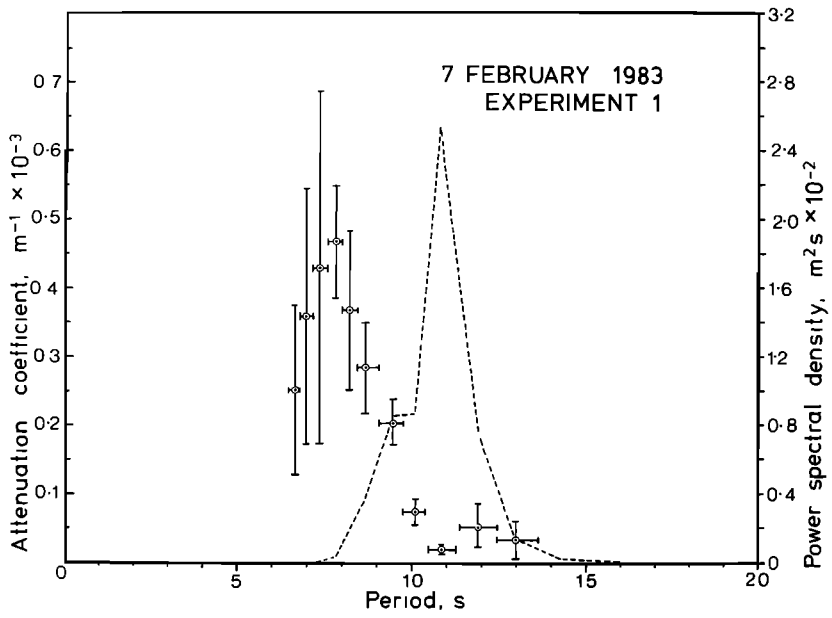

Fig. 11*a*

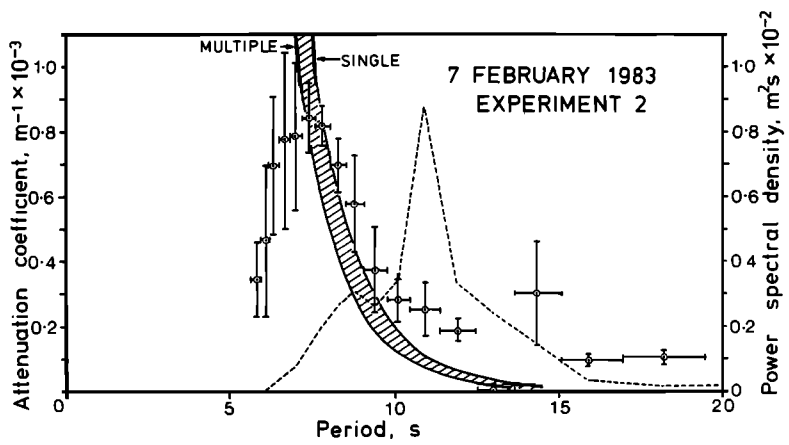

Fig. 11*b*

Fig. 11. Attenuation coefficients as a function of period, and wave spectrum from southernmost site for experiments 1 and 2 on 7 February 1983.

long periods. Within the valid range (10 s to 21 s) the attenuation decreases as the wave period increases. No ice edge measurements of the wave forcing are available since the *Seadisc* buoy was lost in the rough seas. Instead, the most southerly spectrum is plotted to illustrate the energy content of the incident sea near the experimental area. The spectrum consists of a single, but broad, peak at about 14 s period.

4.5. Greenland Sea 1983

26 July. The experimental baseline (figure 3a) covered the entire width of the ice tongue associated with the Fram Strait eddy; by station 6 ice cover changed from close pack into the more open pack of the northern edge of the tongue. Figure 14a shows the energy density against distance (1320 s record length, time step 0.6445 s). It is clear that station 6 is showing regeneration of wave energy, probably due to energy incident from the north, and was therefore disregarded, as was the shipborne station because of problems with buoy calibration. An exponential curve fit was carried out on the remaining five stations giving the results plotted in figure 15; this shows the familiar pattern of α increasing rapidly with frequency and a roll-over at below 8 s period before the incident energy (shown by the spectrum for station 1) becomes too small to permit valid analysis.

29 July. The experimental line (figure 3b) in the direction of the incoming swell was oblique with respect to the ice edge. Therefore any wave refraction occurring at the ice edge will complicate the results. The data were analysed in the same way as for 26 July; figure 14b shows the energy densities, which were very low. Some of the apparent regeneration occurring at high frequencies in the inner stations may actually be a variable noise level in the spectrum, consisting of side lobe leakage from the spectral peaks (further evidence for this came from tests with simulated data, where noise levels of 10^{-5} m^{2}s could easily be generated). Data with energy levels below 10^{-5} m^{2}s were therefore ignored, leaving only three components within a valid range. The computed decay coefficients from seven components are

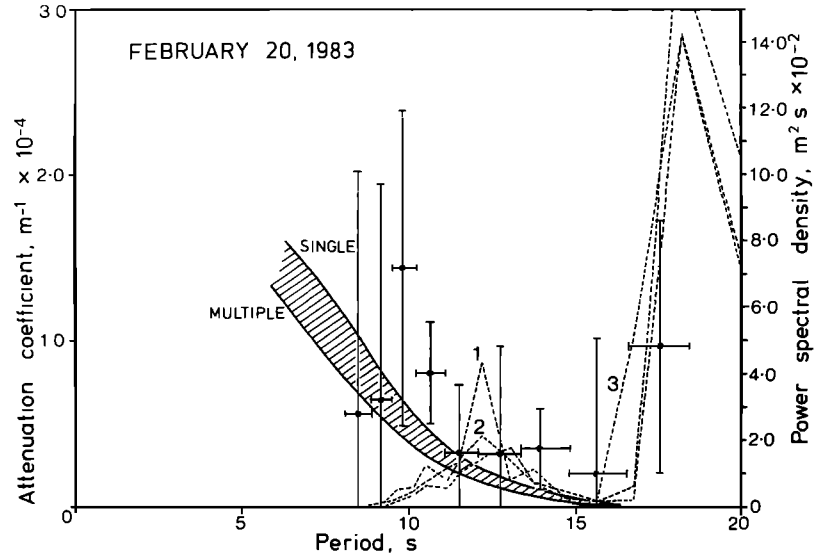

Fig. 12*a*

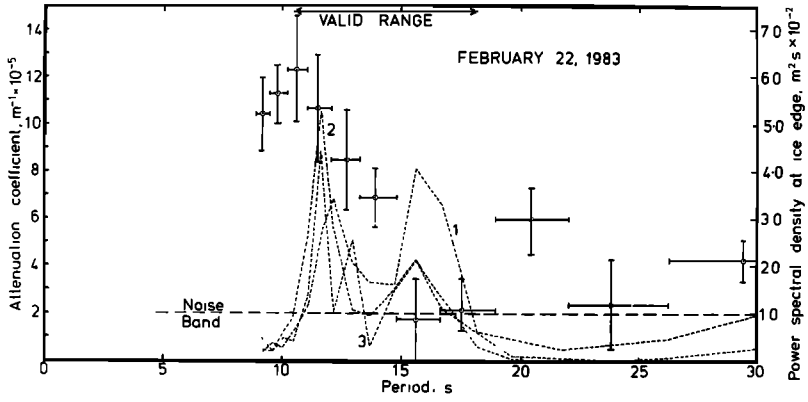

Fig. 12*b*

Fig. 12. Decay coefficients and three open sea spectra for 20 and 22 February 1983.

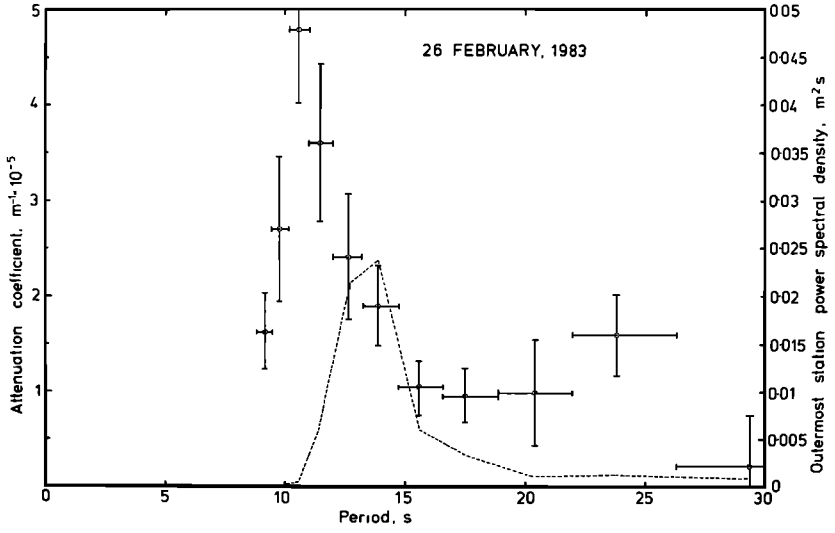

Fig. 13. Attenuation coefficients and southernmost power spectrum, 26 February 1983.

TABLE 2. Computed Attenuation Coefficients for All Wave Experiments Reported in This Paper

Wave Period, s	Frequency Range of Spectral Component, Hz	Energy Attenuation Coefficient α, $m^{-1} \times 10^{-4}$
1978 Greenland Sea: September 16		
12.63	0.0725–0.0859	1.20± 0.16
10.69	0.0868–0.1002	1.92± 0.46
9.28	0.1011–0.1145	4.77± 1.17
8.19	0.1155–0.1288	6.17± 1.46
7.33	0.1298–0.1431	5.28± 1.30
1978 Greenland Sea: September 18		
19.78	0.0439–0.0572	1.95± 0.25
15.41	0.0582–0.0716	1.81± 0.66
12.63	0.0725–0.0859	1.57± 0.67
10.69	0.0868–0.1002	2.35± 0.69
9.28	0.1011–0.1145	3.48± 0.60
8.19	0.1155–0.1288	3.98± 0.47
7.33	0.1298–0.1431	3.34± 0.33
6.63	0.1441–0.1574	2.16± 0.34
6.06	0.1584–0.1717	2.04± 0.29
5.58	0.1726–0.1861	2.61± 0.34
1978 Greenland Sea: September 19		
9.28	0.1011–0.1145	1.21± 0.26
8.19	0.1155–0.1288	1.15± 0.39
7.33	0.1298–0.1431	0.92± 0.23
6.63	0.1441–0.1574	0.66± 0.20
6.06	0.1584–0.1717	0.83± 0.29
5.58	0.1726–0.1861	0.55± 0.20
1978 Greenland Sea: September 21		
12.63	0.0725–0.0859	0.21± 0.10
8.19	0.1155–0.1288	0.46± 0.30
7.33	0.1298–0.1431	1.72± 0.07
6.63	0.1441–0.1574	2.19± 0.17
1978 Greenland Sea: September 22		
10.69	0.0868–0.1002	0.68± 0.18
9.28	0.1011–0.1145	0.84± 0.10
8.19	0.1155–0.1288	0.77± 0.41
7.33	0.1298–0.1431	0.97± 0.67
6.63	0.1441–0.1574	1.09± 0.67
6.06	0.1584–0.1717	1.24± 0.75
5.58	0.1726–0.1861	1.24± 0.69
5.16	0.1870–0.2004	1.06± 0.63
4.81	0.2013–0.2147	1.06± 0.40
1979 Bering Sea: March 11		
14.49	0.063–0.076	0.304± 0.109
12.20	0.076–0.088	0.272± 0.054
10.64	0.088–0.101	0.203± 0.036
9.35	0.101–0.113	0.438± 0.036
8.40	0.113–0.126	0.700± 0.066
7.58	0.113–0.138	0.855± 0.049
6.94	0.138–0.151	0.988± 0.062
6.37	0.151–0.163	1.087± 0.037
5.92	0.163–0.176	1.118± 0.116
5.46	0.176–0.188	1.214± 0.191
5.15	0.188–0.201	1.243± 0.245
4.83	0.201–0.213	1.155± 0.358
1979 Greenland Sea: September 4		
14.03	0.0653–0.0773	0.29± 0.27
11.88	0.0781–0.0902	0.73± 0.25
10.31	0.0910–0.1030	1.23± 0.19
9.10	0.1039–0.1159	2.01± 0.17
8.14	0.1168–0.1288	2.66± 0.22
1979 Greenland Sea: September 10		
11.88	0.0781–0.0902	0.89± 0.46
10.31	0.0910–0.1030	1.25± 0.28
9.10	0.1039–0.1159	1.29± 0.13
8.14	0.1168–0.1288	2.35± 0.54
7.37	0.1297–0.1417	2.37± 1.46
6.73	0.1425–0.1546	2.01± 1.46

TABLE 2. (continued)

Wave Period, s	Frequency Range of Spectral Component, Hz	Energy Attenuation Coefficient α, $m^{-1} \times 10^{-4}$
1983 Bering Sea: February 7 (first experiment)		
12.99	0.0735–0.0805	0.34± 0.26
11.90	0.0805–0.0880	0.55± 0.31
10.87	0.0880–0.0955	0.20± 0.05
10.10	0.0955–0.1025	0.75± 0.19
9.43	0.1025–0.1100	2.05± 0.03
8.77	0.1100–0.1175	2.84± 0.65
8.26	0.1175–0.1245	3.66± 1.16
7.81	0.1245–0.1320	4.66± 0.81
7.35	0.1320–0.1395	4.28± 0.25
6.99	0.1395–0.1465	3.57± 0.18
1983 Bering Sea: February 7 (second experiment)		
12.99	0.0735–0.0805	0.01± 0.89
11.90	0.0805–0.0880	1.89± 0.34
10.87	0.0880–0.0955	2.53± 0.80
10.10	0.0955–0.1025	2.81± 0.64
9.43	0.1025–0.1100	3.76± 1.33
8.77	0.1100–0.1175	5.79± 1.48
8.26	0.1175–0.1245	6.95± 0.81
7.81	0.1245–0.1320	8.17± 0.59
7.35	0.1320–0.1395	8.41± 1.02
6.99	0.1395–0.1465	7.87± 2.67
1983 Bering Sea: February 20		
15.63	0.0605–0.0680	0.20± 0.82
13.89	0.0680–0.0755	0.38± 0.24
12.66	0.0755–0.0830	0.33± 0.63
11.49	0.0830–0.0905	0.36± 0.39
10.64	0.0905–0.0980	0.81± 0.30
9.80	0.0980–0.1035	1.44± 0.94
9.17	0.1035–0.1130	0.65± 1.28
1983 Bering Sea: February 22		
17.54	0.0540–0.0605	0.22± 0.09
15.63	0.0605–0.0680	0.18± 0.17
13.89	0.0680–0.0755	0.68± 0.12
12.66	0.0755–0.0830	0.84± 0.21
11.49	0.0830–0.0905	1.06± 0.23
10.64	0.0905–0.0980	1.23± 0.22
9.80	0.0980–0.1035	1.12± 0.12
9.17	0.1035–0.1130	1.04± 0.15
1983 Bering Sea: February 26		
20.41	0.0455–0.0540	0.10± 0.06
17.54	0.0540–0.0605	0.10± 0.03
15.63	0.0605–0.0680	0.11± 0.03
13.89	0.0680–0.0755	0.19± 0.04
12.66	0.0755–0.0830	0.24± 0.07
11.49	0.0830–0.0905	0.36± 0.08
10.64	0.0905–0.0980	0.48± 0.07
9.80	0.0980–0.1035	0.27± 0.08
9.17	0.1035–0.1130	0.16± 0.04
1983 Greenland Sea: July 26		
15.90	0.0576–0.0682	1.98± 0.20
13.47	0.0689–0.0796	2.87± 0.19
11.68	0.0803–0.0909	4.86± 0.79
10.31	0.0917–0.1023	6.48± 1.05
9.23	0.1030–0.1136	7.35± 0.90
8.35	0.1144–0.1250	8.72± 0.92
7.76	0.1258–0.1364	7.39± 1.46
1983 Greenland Sea: July 29		
10.31	0.0917–0.1023	0.54± 0.05
9.23	0.1030–0.1136	1.42± 0.21
8.35	0.1144–0.1250	3.86± 0.55

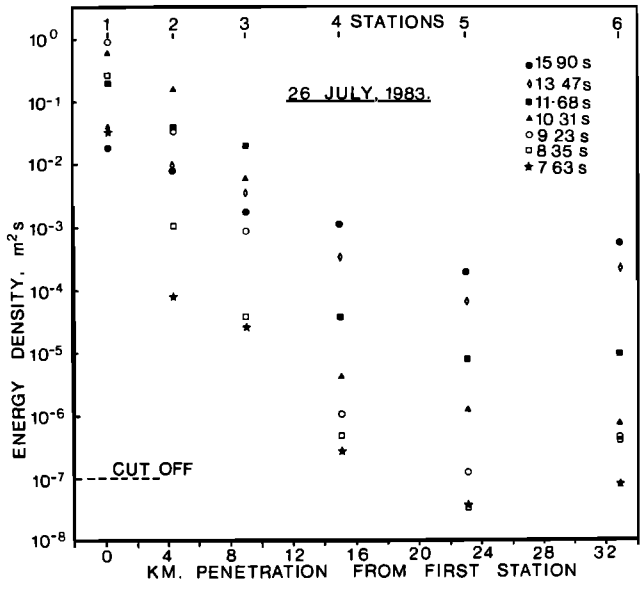

Fig. 14*a*

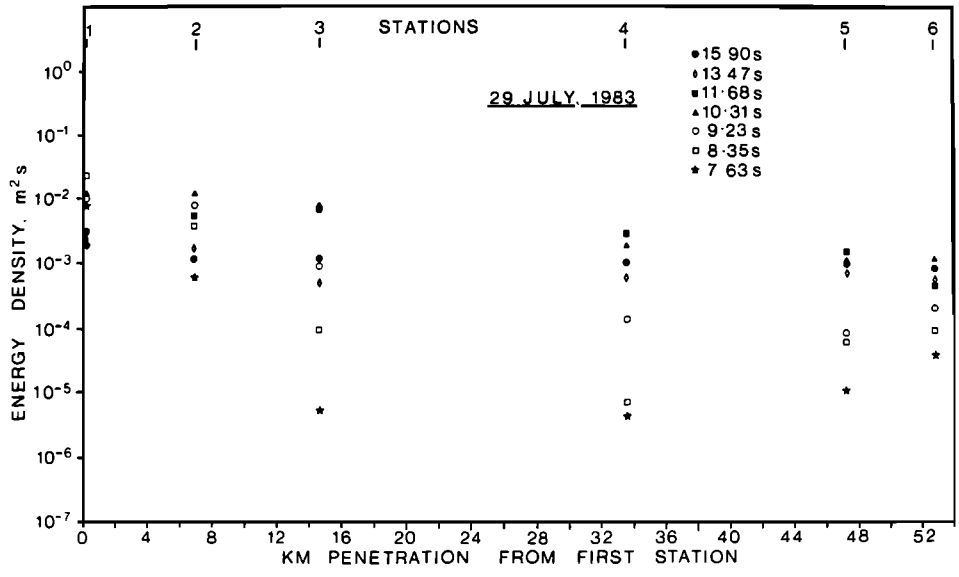

Fig. 14*b*

Fig. 14. Energy densities, 26 and 29 July 1983.

plotted in figure 15, showing the same trend as on 26 July but with much lower decay rates at every frequency. The three attenuation coefficients in the valid range are given in table 2.

5. Conclusions

It has been necessary to plot the results of these many experiments on separate graphs, rather than attempting a universal plot of α against T, because the predictions of the scattering model are critically dependent on the distribution of floe diameters, which is different in every case. Nevertheless, we can draw the following conclusions from these datasets, with the great variety of ice regimes and sea states under which they were obtained giving us some confidence in their general validity:-

1. The attenuation of waves with distance into a pack of discrete ice floes follows a negative exponential, with an attenuation coefficient α which decreases with increasing wave period T over most of the spectral range of medium to long ocean waves.
2. In many cases, the experimental curve of α versus T was observed to possess a roll-over at short periods, whereby the rapid increase in α with decreasing T slows down or even turns into a decrease.
3. A simple one-dimensional model of scattering of waves by individual floes gives predictions which agree well with observations, being especially good in fitting the decrease of α with increasing T which occurs in the mid-range of wind wave periods.
4. The model does not predict the roll-over effect, and in fact predicts that attenuation rates for very short period waves will be so high that such waves should not be seen at all within icefields. This also occurs, incidently, in the model of *Weber* [1987].

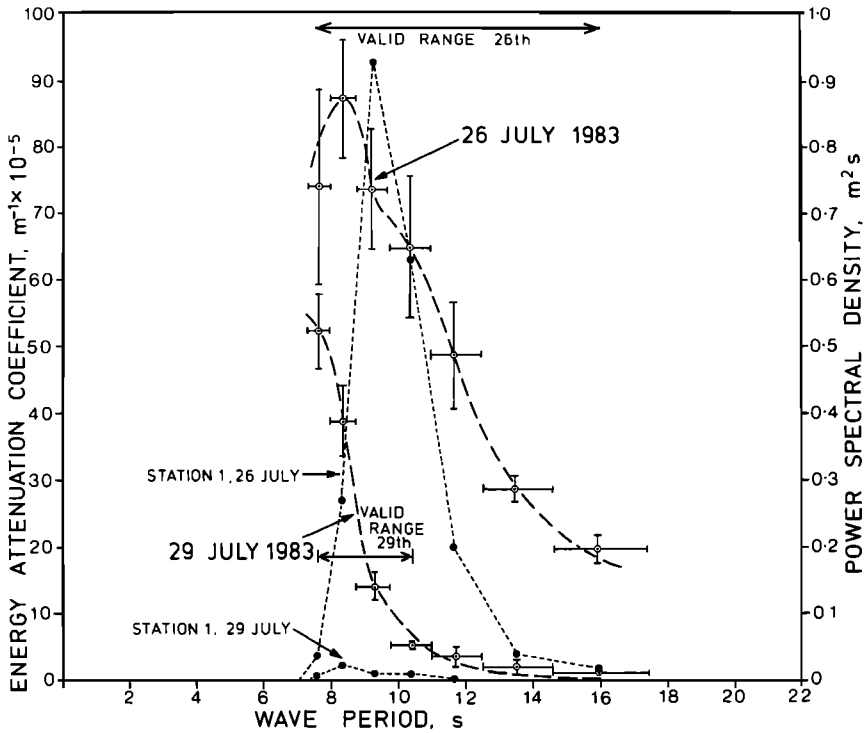

Fig. 15. Decay coefficients and outermost wave spectrum for 26 and 29 July 1983.

5. Two possible explanations for the roll-over effect are
   1. In open icefields, the wind can generate new short wave energy in the open water spaces between floes. A theoretical treatment of wave generation by wind in a sea surface partly covered by floating scatterers is under way (D. Masson, personal commun.).
   2. In concentrated icefields, a non-linear transfer of energy may occur from long to short periods due to the motions induced in ice floes by waves. In other words, floes do not simply scatter waves at the same frequency as the forcing function, but make waves due to such processes as resonant bobbing or pitching, collisions, or rafting events.

The roll-over effect, although not yet treated by theory, is important in that the energy level of short waves in an MIZ icefield is a measure of the level of collisions and other ice floe interactions that are occurring. These, in turn, are a major source of acoustic ambient noise. It is probable, therefore, that short waves and ambient noise levels are strongly correlated, and this has been the subject of recent studies during the MIZEX-87 experiment (P. Rottier, personal commun.).

Acknowledgements. The authors are grateful for continuing support by the US Office of Naval Research, the Natural Environment Research Council of Great Britain, and the British Petroleum Company Ltd. We thank the many scientists who assisted us with the collection of the reported data. We are grateful to Rob Massom for figures, Ruth Weintraub for computing, and Alan Thorndike (University of Puget Sound, Tacoma) for helpful comments.

REFERENCES

Cavalieri, D. J., S. Martin, and P. Gloersen, Nimbus 7 SMMR observations of the Bering Sea ice cover during March 1979, *J. Geophys. Res.*, *88*(C5), 2743–2754, 1983.

Dean, C. H., The attenuation of ocean waves near the open ocean/pack ice boundary, paper presented at Symposium on Antarctic Oceanography, Scientific Committee on Antarctic Research, Santiago, Chile, Sept. 13–16, 1966.

Goodman, D. J., P. Wadhams, and V. A. Squire, The flexural response of a tabular ice island to ocean swell, *Ann. Glaciol.*, *1*, 23–27, 1980.

Johannessen, O. M., W. D. Hibler III, P. Wadhams, W. J. Campbell, K. Hasselmann, and I. Dyer, MIZEX, A program for mesoscale air-ice-ocean interaction experiments in Arctic marginal ice zones, II, A plan for a summer marginal ice zone experiment in the Fram Strait/Greenland Sea, 1984, *Spec. Rep. 83-12*, U.S. Army Cold Reg. Res. and Eng. Lab., Hanover, N. H., 1983.

John, F., On the motion of floating bodies, *Commun. Pure Appl. Math.*, *2*(1), 13–57, 1949.

Overgaard, S., Multi-year sea ice investigation in the East Greenland Current, *Intern. Rep. R228*, Electromagn. Inst., Tech. Univ. Denmark, Lyngby, 1980.

Overgaard, S., P. Wadhams, and M. Leppäranta, Ice properties in the Greenland and Barents seas during summer, *J. Glaciol.*, *29*(101), 142–164, 1983.

Robin, G. de Q., Wave propagation through fields of pack ice, *Philos. Trans. R. Soc. London, Ser. A*, *255*(1057), 313–339, 1963.

Squire, V. A., A preliminary report on field operations in the Bering Sea during Spring 1979, *SPRI Tech. Rep. 79-2*, 27 pp., Scott Polar Res. Inst., Cambridge, England, 1979.

Squire, V. A., Numerical simulation of ice floes in waves, *SPRI Tech. Rep. 81-1*, 57 pp., Scott Polar Res. Inst., Cambridge, England, 1981.

Squire, V. A., Dynamics of ice floes in sea waves, *J. Soc. Underwater Technol.*, *9*(1), 20–26, 1983.

Squire, V. A., and S. Martin, A field study of the physical properties, response to swell, and subsequent fracture of a single ice floe in the winter Bering Sea, *Sci. Rep. 18*, 56 pp., Dep. of Atmos. Sci. and Oceanogr., Univ. of Wash., Seattle, 1980.

Squire, V. A., and S. C. Moore, Direct measurement of the attenuation of ocean waves by pack ice, *Nature*, *283*(5745), 365–368, 1980.

Squire, V. A., P. Wadhams, A. M. Cowan, S. O'Farrell, and R. Weintraub, MIZEX 83 data summary, *SPRI Tech. Rep. 83-1*, 154 pp., Scott Polar Res. Inst., Cambridge, England, 1983.

Stoker, J. J., *Water Waves*, 567 pp., Interscience, New York, 1957.

Wadhams, P., Measurement of wave attenuation in pack ice by inverted echo sounding, in *Sea Ice. Proceedings of an International Conference . . . Reykjavík, Iceland, May 10–13, 1971*, edited by T. Karlsson, pp. 255–260, National Research Council, Reykjavík, Iceland, 1972.

Wadhams, P., The effect of a sea ice cover on ocean surface waves, Ph.D. dissertation, 223 pp., Univ. of Cambridge, England, 1973.

Wadhams, P., Airborne laser profiling of swell in an open ice field, *J. Geophys. Res.*, *80*, 4520–4528, 1975.

Wadhams, P., Wave decay in the marginal ice zone measured from a submarine, *Deep Sea Res.*, *25*, 23–40, 1978.

Wadhams, P., Field experiments on wave-ice interaction in the Labrador and east Greenland currents, 1978, *Polar Rec.*, *19*(121), 373–376, 1979.

Wadhams, P., The seasonal ice zone, in *The Geophysics of Sea Ice*, edited by N. Untersteiner, pp. 825–991, Plenum, New York, 1986.

Wadhams, P., and V. A. Squire, An ice-water vortex at the edge of the East Greenland Current, *J. Geophys. Res.*, *88*(C5), 2770–2780, 1983.

Wadhams, P., S. Martin, O. M. Johannessen, W. D. Hibler III, and W. J. Campbell (Eds.), MIZEX, A program for mesoscale air-ice-ocean interaction experiments in Arctic marginal ice zones, I, Research strategy, *Spec. Rep. 81–19*, U.S. Army Cold Reg. Res. and Eng. Lab., Hanover, N. H., 1981.

Wadhams, P., V. A. Squire, J. A. Ewing, and R. W. Pascal, Directional wave spectra measured near ice edges, in *Proceedings of the Eighth International Conference on Port and Ocean Engineering under Arctic Conditions*, pp. 326–338, Danish Hydraulic Institute, Hørsholm, 1985.

Wadhams, P., V. A. Squire, J. A. Ewing, and R. W. Pascal, The effect of the marginal ice zone on the directional wave spectrum of the ocean, *J. Phys. Oceanogr.*, *16*(2), 358–376, 1986.

Weber, J.E. Wave attenuation and wave drift in the marginal ice zone. Submitted to *J. Phys. Oceanogr.*, 31pp, 6 figs.

A.M. Cowan and S.C. Moore, Polar Oceans Associates, 16 Millers Yard, 10/11 Mill Lane, Cambridge CB2 1RQ, England.

D.J. Goodman, British Petroleum Company Ltd., Britannic House, Moor Lane, London EC2Y 9BU, England.

V.A. Squire, Department of Mathematics and Statistics, University of Otago, PO Box 56, Dunedin, New Zealand.

P. Wadhams, Director, Scott Polar Research Institute, University of Cambridge, Lensfield Road, Cambridge CB2 1ER, England.

(Received April 17, 1986;
accepted February 23, 1987.)